

Calculation of catalyst crust thickness from full elemental laser-induced breakdown spectroscopy images

L Sorbier¹, F Trichard², S Moncayo³, C P Lienemann¹ and V Motto-Ros³

¹ IFP Energies nouvelles, Rond-point de l'échangeur de Solaize, P.O. Box 3, 69360 Solaize, France

² Ablatom SAS, Bâtiment Kastler, Domaine Scientifique de la Doua, 10 rue Ada Byron, 69622 Villeurbanne Cedex, France

³ Institut Lumière Matière UMR 5306, Université Lyon 1 - CNRS, Université de Lyon, 69622 Villeurbanne Cedex, France

E-mail: loic.sorbier@ifpen.fr

Abstract. We propose a methodology to compute the crust thickness of an element in an egg-shell catalyst from a two-dimensional elemental map. The methodology handles two important catalyst shapes: infinite extrudates of arbitrary section and spheres. The methodology is validated with synthetic analytical profiles on simple shapes (cylinder and sphere). Its relative accuracy is shown close to few percent with a decrease inversely proportional to the square root of the number of sampled pixels. The crust thickness obtained by this method from quantitative Pd maps acquired by laser-induced breakdown spectroscopy are comparable with values obtained from electron-probe microanalysis profiles. Some discrepancies are found and are explained by the heterogeneity of the crust thickness within a grain. As a full map is more representative than a single profile, fast mapping and the methodology exposed in this paper are expected to become valuable tools for the development of new generations of egg-shell deposited catalysts.

1. Introduction

Selective hydrogenation is an important process in petrochemistry. The process is employed for the stabilisation of pyrolysis gasoline and vapocacking products. For either processes, the unsaturated carbon-carbon bonds need to be partially hydrogenated. Conjugated double bonds or triple bonds should be removed while keeping intact non-conjugated double bonds. To obtain a good activity and selectivity, heterogeneous catalysts are employed. These catalysts have the shape of cylinders or multilobed extrudates or are nearly spherical pellets. Typical sizes of grains are around a few millimetres. The catalyst support is often composed of a chemically inert oxide such as alumina, silica or titanium oxide. Active phases are noble metals (Pd, Ag, Au) deposited on the support at concentration ranging from 0.1 to 0.5 wt%. As hydrogenation of carbon bonds has a very fast kinetics, these catalysts are working in internal diffusion limited regime: chemical kinetics occur quicker than diffusion of products in the grain.

For catalysts under strong internal diffusion regime, the distribution of active element along the pellets diameter is correlated with the catalyst performance. Therefore, for selective hydrogenation catalysts, noble metals are deposited as an egg-shell distribution on the support, otherwise said on a



crust close to grain's surface. This crust enhances the activity and selectivity and limits the deactivation rate compared to flat repartition of the active element. It is therefore important to have adequate characterisation techniques to check the deposit of metals at the grain scale. For palladium selective hydrogenation catalyst, a descriptor, the Pd crust thickness, has been defined and correlated with hydrogenation activity. This crust thickness was calculated from elemental profiles obtained by electron probe microanalysis (EPMA) and trivial pellet shapes (slab, cylinder, sphere). It is defined as the thickness of the crust containing a fixed proportion (80 % or 98 %) of the total Pd content in the grain. As alumina supports are white and deposited Pd appears darker, a crust thickness may also be evaluated by optical microscopy and image analysis. This method, however, is impeded to the optical visibility of the crust and the definition of this crust thickness is not based on a quantitative Pd content criterion.

The methodology exposed in reference does not handle multilobed shapes used for some industrial processes. Using a proper strategy based on the distance transform, long extrudates of arbitrary simply connected section should however be handled. Besides, optical micrographs of catalyst cross-sections clearly show that the Pd deposits are often irregular. A single profile along the grain's cross-section is then less representative of the catalyst batch than a full two-dimensional (2D) map of the section of the grain. The interest of using 2D mapping is increased by the development of fast laser-induced breakdown spectroscopy (LIBS) mapping. LIBS allows to acquire elemental maps of materials with a lateral resolution of a few micrometres at a sampling rate of 1 to 1,000 points per second. The reviews of Kaiser *et al.* for biological applications and Piñon *et al.* for material science give a good sight of the possibilities and drawbacks of the technique. One of the drawbacks of LIBS is that it needs a proper calibration strategy. There is no universal correction procedure like for EPMA. We have recently proposed to calibrate the intensities measured by LIBS with concentrations obtained by EPMA on the same profiles acquired with the same lateral resolution. It leads to quantitative mapping with a lower limit of detection (about 4 times) and higher speed (about 240 times) compared to EPMA. This opens the possibility to compute crust thicknesses from 2D elemental maps.

Nevertheless, computing the crust thickness on 2D map of a 3D object may not be straightforward as for example, for a 2D map of a spherical grain. The aim of this paper is then to propose a convenient strategy for computing crust thickness from 2D elemental map of a catalyst grain for two important catalyst pellet shapes of industrial importance: long extrudates and spherical grains. The paper is organised as follows. In a first section, we summarise the experimental methods: synthesis of the alumina supported Pd catalyst and analysis methods by EPMA and LIBS. The calculation of the quantity of an element contained at a given distance to the grain's border is discussed for two important shapes: infinitely long extrudates and spherical grains. The algorithm to compute the crust thickness from 2D maps is then proposed. The section ends up with the calculation of crust thickness from empirical analytical concentration fields on simple shapes (slabs, cylinder, sphere). The second section is devoted to the presentation of results: accuracy of the methodology on analytical profiles, 2D Pd LIBS maps, EPMA profiles and comparison of crust thickness measured either from profiles or from full maps. We close with a discussion and a conclusion.

2. Materials and methods

2.1. Pd hydrogenation catalyst

Synthesis of Pd catalyst was done by incipient wetness impregnation of an aqueous solution of palladium nitrate to target a 0.274 wt% Pd content. Details of the catalyst preparation can be found in reference. Catalyst beads were embedded in conductive resin (Struers Polyfast), polished with SiC paper under water solvent up to their diameter and finished with a 1 μm diamond suspension.

2.2. Analysis by EPMA

A 20-nm thick carbon layer was coated on the sample before EPMA analysis. EPMA analysis was performed on a JEOL JXA 8100 fitted with five wavelength-dispersive X-ray spectrometers. The electron beam (20 kV, 240 nA) was defocussed to obtain a 15 μm diameter probe. The measurement times on peak and background on each point was set to 20 s. Oxygen was dosed using a stoichiometric method assuming metallic Pd and Al_2O_3 oxide. Pure Pd (Goodfellow, wire 99.95 % purity) and pure alumina (Goodfellow, sapphire pellet diameter 3 mm, 99.9 % purity) were used as standards. Profiles along the beads diameters were acquired with a 15 μm step. The first and last points of the profiles were in the surrounding resin to ensure a full diameter measurement. In these conditions, a profile lasted about 70 minutes with a detection limit at 84 ppm for Pd. Three profiles on three different catalyst grains of the same batch were acquired. From each profile, the crust thickness is calculated using the method described in reference 0 assuming a spherical shape.

2.3. Analysis by LIBS

Before LIBS analysis, the sample was slightly polished and finished with 1 μm diamond suspension in order to remove the carbon coating. LIBS analysis was performed on a system dedicated to LIBS imaging that has been described in detail elsewhere 0. The laser source, a Nd:YAG was used at the fundamental wavelength (1,064 nm) at a 10 Hz repetition rate. The typical pulse energy after shaping and attenuation was set to 600 μJ .

The plasma radiation was collected with a lens-fibre system positioned at a take-off angle of 35°. The collected light was analysed using a Czerny-Turner spectrometer (Shamrock 303, Andor Technology) fitted with an intensified charge-coupled device camera (iStar ICCD, Andor Technology). The intense Pd(I) 340.45 nm and less intense Pd(I) 343.34 nm lines were used for quantitative imaging. Two calibration curves for these lines were constructed from the same analysis points acquired on the same sample using intensities of LIBS and local concentration of EPMA. The calibration curve of Pd (I) 340.45 nm line was used for low local Pd contents ($c \leq 0.1$ wt%) and the one of Pd(I) 343.34 nm for high local Pd content ($c > 0.1$ wt%). Maps of 250×210 pixels with a 15 μm resolution were acquired on the same three catalyst grains as EPMA was conducted on, each mapping lasting about 90 minutes with a detection limit of 18 ppm for Pd.

2.4. From concentration map to crust thickness

2.4.1. General equation. Let $c(x, y, z)$ be the concentration field of an element on the grain G . Let M be the mask of the grain. The mask M is computed by binarisation of the concentration map of an element contained in catalyst but not in surrounding resin (Pd). The distance transform of the mask M^{DT} is computed 0. It contains in each pixel, the distance (in pixels) from the border of the mask. For pixels outside the mask, the distance transform is equal to zero. Let K be the maximum distance to the border of the mask, $K = \max M^{\text{DT}}$.

The quantity $q(a, b)$ of the element contained at a distance from the border of the grain comprised between a and b is equal to:

$$q(a, b) = \iiint_G \chi_{a,b}(x, y, z) c(x, y, z) \rho(x, y, z) dx dy dz \quad (1)$$

where $\chi_{a,b}(x, y, z)$ is an indicator function equal to one if the point of coordinates (x, y, z) lies at a distance comprised between a and b from the border of grain and ρ is the volumic mass.

2.4.2. Infinitely long extrudate. For an infinite long extrudate having its extrusion axis on axis z , neither the concentration field nor the indicator function depends on z . Besides, the concentration field is only sampled on a finite number of pixels such that eq. (1) is evaluated using rectangle method. Hence, if we suppose that $\rho(x, y, z)$ is constant, the quantity of element by unit length along z axis is equal to:

$$q_E(np, (n+1)p) \approx p^2 \rho \sum_{(x_i, y_i)} \chi_{np, (n+1)p}(x_i, y_i) c(x_i, y_i) \quad (2)$$

where n is an integer and p the pixel size. Yet, the indicator function $\chi_{np, (n+1)p}(x, y)$ is related with M^{DT} the distance transform of the mask of the grain, namely we have $\chi_{np, (n+1)p}(x, y) = \delta(M^{DT}(x, y) - np)$ with δ the Dirac function. Hence:

$$q_E(np, (n+1)p) \approx p^2 \rho \sum_{(x_i, y_i)} \delta(M^{DT}(x_i, y_i) - np) c(x_i, y_i) \quad (3)$$

2.4.3. Sphere. For a sphere of radius R where the concentration field is sampled on a plane containing the centre of the sphere, and a radial symmetric concentration field, the quantity of an element at a distance between a and b from the border of the grain is:

$$q_S(a, b) = \rho \int_0^R \chi_{a,b}(r) c(r) 4\pi r^2 dr \quad (4)$$

Let $x = r \cos \theta$ and $y = r \sin \theta$, since $r = \sqrt{x^2 + y^2}$ and $dx dy = r dr d\theta$, we have:

$$\begin{aligned} q_S(a, b) &= \rho \int_0^R \int_0^{2\pi} \chi_{a,b}(r) c(r) 2r d\theta r dr \\ &= 2\rho \iint_{x^2+y^2 \leq R^2} \chi_{a,b}(x, y) c(x, y) \sqrt{x^2 + y^2} dx dy \end{aligned} \quad (5)$$

The concentration field is only sampled in a finite number of pixels such that rectangle method gives:

$$q_S(np, (n+1)p) \approx 2p^2 \rho \sum_{(x_i, y_i)} \chi_{np, (n+1)p}(x_i, y_i) c(x_i, y_i) \sqrt{x_i^2 + y_i^2} \quad (6)$$

As $\chi_{np, (n+1)p}(x, y) = \delta(M^{DT}(x, y) - np)$ and at a given distance np to the border of the grain, $\sqrt{x_i^2 + y_i^2}$ is constant and approximately equal to $\frac{p}{2\pi} \sum_{(x_i, y_i)} \delta(M^{DT}(x_i, y_i) - np)$, we obtain:

$$q_S(np, (n+1)p) \approx \frac{p^3 \rho}{\pi} \left(\sum_{(x_i, y_i)} \delta(M^{DT}(x_i, y_i) - np) \right) \left(\sum_{(x_i, y_i)} \delta(M^{DT}(x_i, y_i) - np) c(x_i, y_i) \right) \quad (7)$$

2.5. Calculation of crust thickness

Let set $\Delta Q_F(k) = q_F((k-1)p, kp)$, where $F = E$ for an extrudate or $F = S$ for a sphere, be the quantity of the element at a distance between $(k-1)p$ and kp from the border of the grain. The crust thickness t_X , defining the distance to the border of the grain containing the proportion X of an element is computed in five steps:

1. From the concentration map, compute the mask M of the grain and its distance transform M^{DT} ;
2. Compute the quantity of the element at a distance between $(k-1)$ and k pixels from the border of the grain $\Delta Q_F(k)$ for each distance $k \in \{0, \dots, K\}$ using either eq. (3) for a cylinder or eq. (7) for a sphere;
3. Compute the relative proportion of element present at a distance lower than k pixels from the border of the grain $Q_F(k) = \frac{\sum_{i=0}^k \Delta Q_F(i)}{\sum_{i=0}^K \Delta Q_F(i)}$ for each distance $k \in \{0, \dots, K\}$;
4. Search for the distances k_0 and $k_0 + 1$ in pixels which are bracketing the relative quantity X : look for k_0 in $\{0, \dots, K-1\}$ such that $Q_F(k_0) \leq X < Q_F(k_0 + 1)$;
5. Compute the crust thickness in pixels with sub-pixel accuracy by linear interpolation and convert it in physical unit length by the use of pixel size: $t_X = p \left(k_0 + \frac{X - Q_F(k_0)}{Q_F(k_0 + 1) - Q_F(k_0)} \right)$.

2.6. Accuracy estimation from analytical concentration fields

The calculation of crust thickness from a synthetic analytical concentration field on simple shapes (infinite cylinder, sphere) may help to validate the approach and estimate the accuracy of the method.

Suppose that the concentration field does only depends on the distance to the border of the grain, consequently to the distance to the centre of the grain r . We also suppose that the concentration field $c_m(r)$ obeys the following law:

$$c_m(r) = \left(\frac{r}{R}\right)^m \quad (8)$$

where R is the radius of the grain and $m \geq 1$ is a real. Such concentration field leads to hollow profiles for $m \geq 1$. The relative quantity of element $Q_m^n(y)$ contained in a ball of radius y in \mathbb{R}^n ($n = 2$ infinite cylinder, $n = 3$ sphere) is equal to:

$$Q_m^n(y) = \frac{\int_0^y c_m(r) dV^n(r)}{\int_0^R c_m(r) dV^n(r)} \quad (9)$$

where $dV^n(r)$ is the infinitesimal volume in \mathbb{R}^n . Replacing the expression of $c_m(r)$ of eq. (8) and as $dV^n(r) = \pi^{\frac{n}{2}} \Gamma\left(\frac{n}{2} + 1\right)^{-1} n r^{n-1} dr$ we obtain:

$$Q_m^n(y) = \frac{y^{m+n}}{R^{m+n}} \quad (10)$$

The crust thickness $T_m^n(X)$ is defined as the thickness of the corona of external radius R and internal radius $R - T_m^n(X)$ which contains the relative fraction X of the element. The ball of radius $R - T_m^n(X)$ should then contain the relative quantity $1 - X$. Therefore, using eq. (10), $T_m^n(X)$ is the solution of:

$$1 - X = \frac{[R - T_m^n(X)]^{m+n}}{R^{m+n}} \quad (11)$$

and we obtain:

$$\frac{T_m^n(X)}{R} = 1 - (1 - X)^{\frac{1}{m+n}} \quad (12)$$

To evaluate the accuracy of the algorithm proposed in section 2.5, we simulate a concentration map following the eq. (8) on a ball of radius R with a pixel size p . On the synthetic concentration map we calculate t_X using the algorithm exposed in section 2.5. We define the relative error ε_t by:

$$\varepsilon_t = \frac{|t_X - T_m^n(X)|}{T_m^n(X)} \quad (13)$$

3. Results

3.1. Accuracy on analytical profiles

To evaluate the accuracy of the algorithm proposed in section 2.5, we have calculated the crust thickness for different values of the parameter m for $R = 1.5$ mm and $p = 15$ μ m. The results of the algorithm are compared to the theoretical value given by eq. (12) in figure 1. The relative error given by equation (13) is then computed and presented in figure 2.

The influence of the number of pixels n_p employed to sample the concentration field is shown in figure 3 for a value of $m = 10$. This value of m gives a relative crust thickness ($t_{98\%}/R$) close to the one measured in section 3.2. Relative errors for a cylinder and sphere shapes are both decreasing inversely proportional to the square root of the number of pixels n_p .

3.2. Crust thickness from LIBS Pd maps and EPMA profiles

Figure 4 shows the quantitative LIBS Pd maps for the three sampled catalyst grains and figure 5 the EPMA profiles on these same grains. We notice a clear egg-shell repartition of Pd. LIBS maps show a rather heterogeneous distribution of Pd in the crust among grains and even within the same grain.

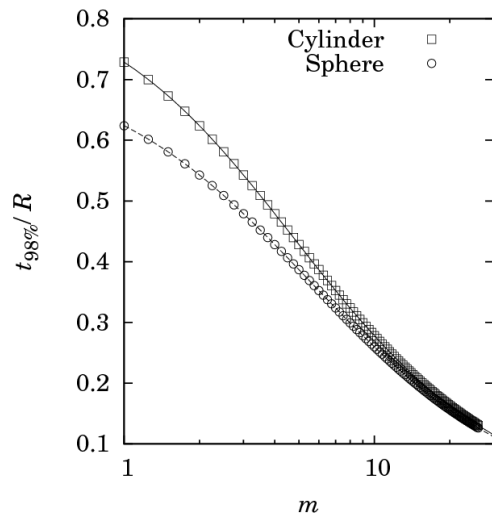


Figure 1. Crust thickness computed by algorithm of section 2.5 (symbols) compared to theoretical value of eq. (12) (lines).

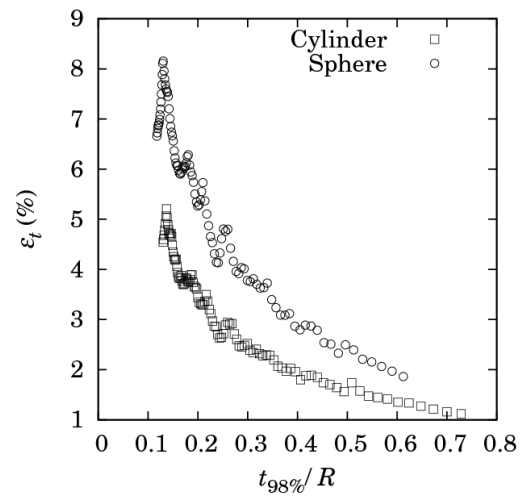


Figure 2. Relative error in function of crust thickness for $R = 1.5$ mm, $p = 15$ μ m and a concentration field following eq. (8).

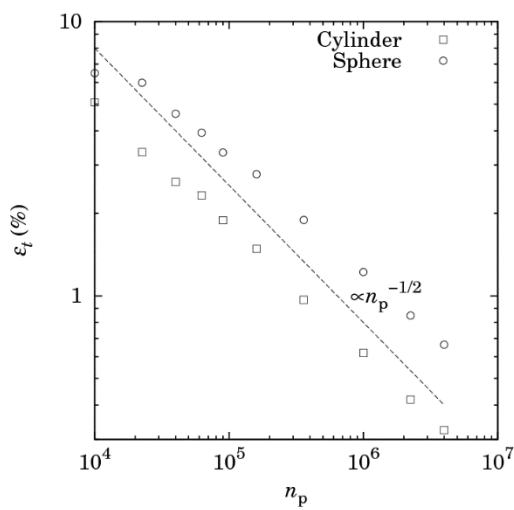


Figure 3. Relative error of $t_{98\%}$ for $m = 10$. The dotted line is decreasing as $n_p^{-1/2}$.

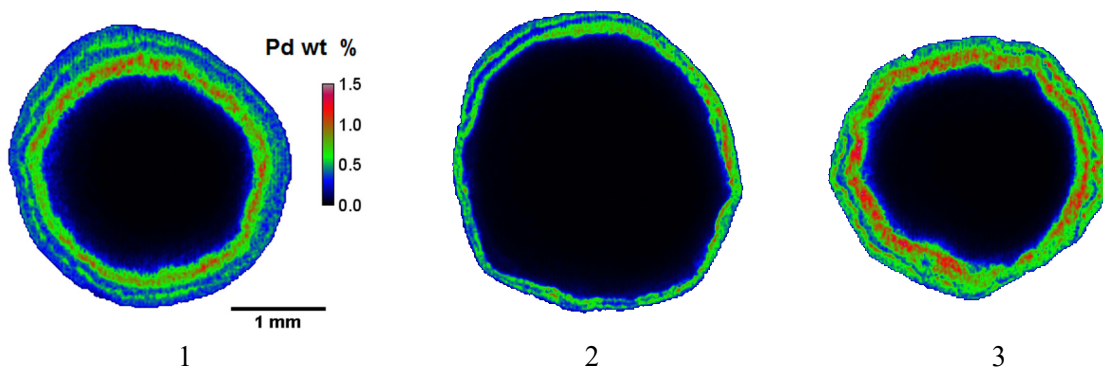


Figure 4. LIBS Pd maps for the 3 sampled grains.

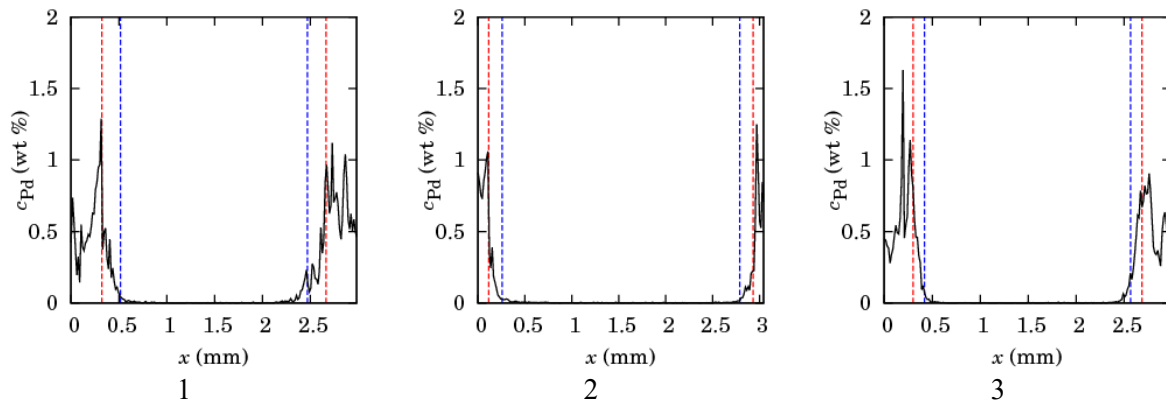


Figure 5. EPMA Pd profiles along the diameter of the 3 sampled grains. Dotted lines show crust thicknesses $t_{80\%}$ (red) and $t_{98\%}$ (blue).

Table 1 reports the crust thickness measured either from profiles (EPMA) or from 2D maps (LIBS) on the three sampled grains. Comparison between the two methods are shown in figure 6.

Table 1. Crust thickness measured on profiles by EPMA and on maps by LIBS for the three catalyst grains.

Grain	$t_{80\%}$		$t_{98\%}$	
	EPMA	LIBS	EPMA	LIBS
1	320	337	516	531
2	113	166	257	406
3	300	262	419	423

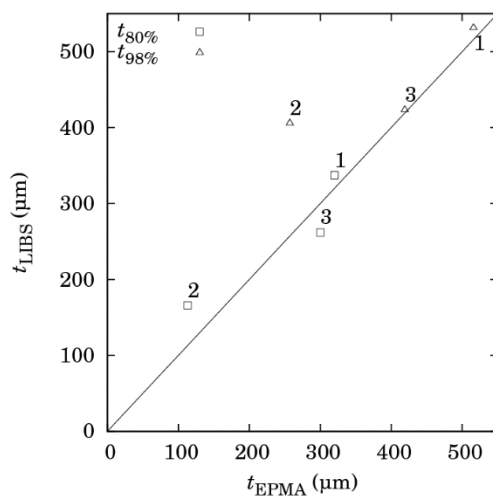


Figure 6. Thickness measured from profiles (EPMA) and from 2D maps (LIBS). Numbers identify grain number. The straight line is the first bisector.

4. Discussion

Figure 1 shows that the algorithm proposed is a good estimator of the crust thickness, from slightly hollow profiles (small values of parameter m , thick crust) to very hollow profiles (high values of

parameter m , thin crust). Figure 2 clearly shows that the relative accuracy increases when the crust thickness decreases (high value of the parameter m). This is explained by the poor sampling of the concentration field where the concentration is appreciable (when m is large). Figure 3 confirms this explanation. For a fixed profile, increasing the number of points on the concentration map decreases the relative error. The decrease is inversely proportional to the square root of the number of points, which is expected for the two-dimensional rectangle method (see Appendix A). Besides, figure 3 shows that the proposed methodology converges to the expected value, otherwise said that we have proposed an unbiased estimator of the crust thickness. The accuracy predicted for geometry and crust thickness close to the experimental one of figure 4 is in the order of a few percent. This is quite acceptable as it is the same order of magnitude than the accuracy of the measure of apparent activity of a catalyst.

The comparison of crust thickness obtained from 2D LIBS maps with the reference values obtained from EPMA profiles shows an overall good agreement. Discrepancies between the two methods are observed for the grain 2. This grain has the thinnest and less regular crust (see figure 4). It is worth noticing that the crust thickness calculation from a 2D map is more representative than the one calculated from a single profile. The reference values obtained from EPMA profiles are then less reliable than the one calculated from LIBS maps. Interaction volumes are slightly different between EPMA and LIBS. For an alumina with 60 % porosity at 20 kV, the analysis volume is in the order of 5 μm large and 5 μm deep. Since a defocused probe of 15 μm diameter was used, the analysis volume is about 1,500 μm^3 . With the laser conditions employed in this work, LIBS leads to crater sizes of about 10 μm large by 2.5 μm deep thus to an analysed volume of about 200 μm^3 . LIBS probes a smaller volume (due to the electron probe defocus) but both lateral resolutions are comparable and well below the measured crust thicknesses.

We now want to compare the advantages and limitations of the three methodologies available to compute the crust thickness of a catalyst: from elemental 2D maps as proposed in this paper, from profiles, and from optical microscopy. It is clear that the use of 2D information (elemental or optical) is more representative than a single profile. The main drawback of optical microscopy is that it is restricted to a visible crust, in other words to elements colouring an uncoloured catalyst support. The definition of crust thickness from optical microscopy is also questionable for low active phase concentrations. The advantage of optical microscopy is the speed of the process (about 10 minutes per sample). The main drawback of the calculation of crust thickness from a 2D map is the long acquisition time of the map. This methodology should therefore be reserved to fast and sensitive analytical techniques. Fortunately, fast LIBS mapping at 10 Hz already leads to a map acquisition time (90 minutes) close to one EPMA profile acquisition time (70 minutes) and with a better limit of detection. Some LIBS mapping systems with a 100 Hz sampling rate already exists and sampling rates of 1 kHz are conceivable in the future. This will enhance the interest of the methodology we have proposed in this paper. This methodology and such fast mapping techniques should reduce the development times of new generations of egg-shell catalysts.

5. Conclusion

We have proposed a methodology to compute the crust thickness of an egg-shell catalyst from 2D elemental maps. This method handles important industrial catalyst shapes: long extrudates of arbitrary section and spheres. This methodology has been validated by analytical synthetic profiles for simple shapes (cylinder and sphere). We have shown that the proposed estimator is unbiased and converge to the true crust thickness value with an error inversely proportional to the square root of the number of sampled pixels.

We have demonstrated the applicability on real data obtained from quantitative LIBS mapping. The calibration of the LIBS intensities has been obtained from EPMA performed with the same lateral resolution on the same profiles of a sample. Comparisons of crust thickness calculated from LIBS 2D maps with the ones calculated from EPMA profiles show a satisfactory agreement except for irregular

crust where profiles lack representativeness. The methodology presented in this paper is going to be a valuable tool for the development of new generations of egg-shell catalysts thanks to the development of fast LIBS mapping.

Appendix A. Error bound for rectangle rule

Let $f : \mathbb{R}^2 \rightarrow \mathbb{R}$, $(x, y) \mapsto f(x, y)$, a function that we suppose continuous, locally summable and 1-differentiable. We want to integrate f on the domain $D = [x_1; x_n] \times [y_1; y_n]$. The integration error $\varepsilon_{i,j}$ for the rectangle method on the pixel (x_i, y_j) is:

$$\varepsilon_{i,j} = \left| \int_{x_i}^{x_{i+1}} \int_{y_j}^{y_{j+1}} (f(x, y) - f(x_i, y_j)) dx dy \right| \quad (\text{A1})$$

Obviously:

$$\varepsilon_{i,j} \leq \int_{x_i}^{x_{i+1}} \int_{y_j}^{y_{j+1}} |f(x, y) - f(x_i, y_j)| dx dy \quad (\text{A2})$$

Now, right hand side of (A2) lets appear the first term of the Taylor expansion of f . It is possible to have the Lagrange remainder of this Taylor expansion, more precisely $\forall (x, y) \in [x_i; x_{i+1}] \times [y_j; y_{j+1}] \exists (x_\xi, y_\xi) \in [x_i; x_{i+1}] \times [y_j; y_{j+1}]$ so that 0:

$$f(x, y) = f(x_i, y_j) + \frac{\partial f}{\partial x}(x_\xi, y_\xi)(x - x_i) + \frac{\partial f}{\partial y}(x_\xi, y_\xi)(y - y_j) \quad (\text{A3})$$

Injecting (A3) into (A2) and considering that $|a + b| \leq |a| + |b|$ we obtain:

$$\varepsilon_{i,j} \leq \int_{x_i}^{x_{i+1}} \int_{y_j}^{y_{j+1}} \left(\left| \frac{\partial f}{\partial x}(x_\xi, y_\xi)(x - x_i) \right| + \left| \frac{\partial f}{\partial y}(x_\xi, y_\xi)(y - y_j) \right| \right) dx dy \quad (\text{A4})$$

Now, we suppose that f is sufficiently regular to have its first derivative bounded in D so that $\forall (x, y) \in D, \exists K \in \mathbb{R}^+, \left| \frac{\partial f}{\partial x}(x, y) \right| \leq K$ and $\left| \frac{\partial f}{\partial y}(x, y) \right| \leq K$. Taking into account that $(x - x_i) \geq 0$ and $(y - y_j) \geq 0$ in (A4) we have:

$$\varepsilon_{i,j} \leq K \int_{x_i}^{x_{i+1}} \int_{y_j}^{y_{j+1}} [(x - x_i) + (y - y_j)] dx dy \quad (\text{A5})$$

The integral in right hand side of (A5) may be explicitly calculated. Setting $x_{i+1} = x_i + p$ and $y_{i+1} = y_i + p$, p being the pixel size, we obtain:

$$\varepsilon_{i,j} \leq \frac{K}{2} p^3 \quad (\text{A6})$$

The error of integration in D , ε writes:

$$\varepsilon \leq \sum_{i=1}^n \sum_{j=1}^n \varepsilon_{i,j} \quad (\text{A7})$$

Injecting (A6) into (A7) and using the relations $np = x_n - x_1 = y_n - y_1$ and $n_p = n^2$, we obtain:

$$\varepsilon \leq \frac{K (x_n - x_1)^3}{2 n_p^{1/2}} \quad (\text{A8})$$

with n_p the number of pixels. The observed behaviour in figure 3 of the paper is recovered.

References

- [1] Shadman-Yazdi F and Petersen E 1972 *Chem. Engng. Sci.* **27** 227-237
- [2] Berenblyum A, Mund S, Karelskii V, Goranskaya T, Zolotukhin V and Lakhman L 1986 *Kinet. Catal.* **27** 184-187
- [3] Lin T B and Chou T C 1994 *Appl. Catal. A* **108** 7-19
- [4] Sorbier L, Gay A-S, Fécant A, Moreaud M and Brodusch N 2012 *IOP Conf. Ser. Mater. Sci. Engng.* **32** 012023

- [5] Sorbier L, Gay A-S, Fécant A, Moreaud M and Brodusch N 2013 *Microsc. Microanal.* **19** 293–299
- [6] Sorbier L, Bazer-Bachi F, Blouët Y, Moreaud M and Moizan-Basle V 2016 *Microsc. Microanal.* **22** 422-431
- [7] Kaiser J, Novotný K, Martin M, Hrdlička A, Malina R, Hartl M and Kizek R 2012 *Surf. Sci. Rep.* **67** 233-243
- [8] Piñon V, Mateo M and Nicolas G 2013 *Appl. Spectrosc. Rev.* **48** 357-383
- [9] Trichard F, Sorbier L, Moncayo S, Blouët Y, Lienemann C P and Motto-Ros V 2017 *Spectrochim. Acta B* **133** 45-51
- [10] Motto-Ros V, Negre E, Pelascini F, Panczer G and Yu J 2014 *Spectrochim. Acta B* **92** 60-69
- [11] Rosenfeld A and Pfaltz J 1966 *J. ACM* **13** 471-494
- [12] Sommerville D 1929 *An introduction to the geometry of n dimensions*. (London: Methuen and Co.) 136
- [13] Cáceres J, Pelascini F, Motto-Ros V, Moncayo S, Trichard F, Panczer G, Marín-Roldán A, Cruz J, Coronado I and Martín-Chivelet J 2017 *Sci. Rep.* **7** 5080
- [14] Coleman R 2012 *Calculus on normed vector spaces*. (New York: Springer) 111